



Article

Tunable Broadband Solar Energy Absorber Based on Monolayer Transition Metal Dichalcogenides Materials Using Au Nanocubes

Jiakun Li ^{1,†}, Zeqiang Chen ^{2,†}, Hua Yang ³ , Zao Yi ^{1,*} , Xifang Chen ^{1,*}, Weitang Yao ¹, Tao Duan ¹, Pinghui Wu ^{2,*}, Gongfa Li ⁴ and Yougen Yi ⁵

¹ Joint Laboratory for Extreme Conditions Matter Properties, Southwest University of Science and Technology, Mianyang 621010, China; lijiaokun1999@yeah.net (J.L.); wtyao@ustc.edu.cn (W.Y.); myyz1984@swust.edu.cn (T.D.)

² Research Center for Photonic Technology, Fujian Key Laboratory for Advanced Micro-nano Photonics Technology and Devices & Key Laboratory of Information Functional Material for Fujian Higher Education, Quanzhou Normal University, Fujian 362000, China; czqchem@qztc.edu.cn

³ State Key Laboratory of Advanced Processing and Recycling of Non-ferrous Metals, Lanzhou University of Technology, Lanzhou 730050, China; hyang@lut.cn

⁴ Key Laboratory of Metallurgical Equipment and Control Technology of Ministry of Education, Wuhan University of Science and Technology, Wuhan 430081, China; ligongfa@wust.edu.cn

⁵ College of Physics and Electronics, Central South University, Changsha 410083, China; yougenyi@csu.edu.cn

* Correspondence: yizaomy@swust.edu.cn (Z.Y.); chenxifang1988@yeah.net (X.C.); phwu@zju.edu.cn (P.W.); Tel./Fax: +86-0816-2480872 (Z.Y.); +86-0816-2480872 (X.C.); +86-0595-22003815 (P.W.)

† These authors contribute equally to this work.

Received: 3 January 2020; Accepted: 31 January 2020; Published: 1 February 2020



Abstract: In order to significantly enhance the absorption capability of solar energy absorbers in the visible wavelength region, a novel monolayer molybdenum disulfide (MoS₂)-based nanostructure was proposed. Local surface plasmon resonances (LSPRs) supported by Au nanocubes (NCs) can improve the absorption of monolayer MoS₂. A theoretical simulation by a finite-difference time-domain method (FDTD) shows that the absorptions of proposed MoS₂-based absorbers are above 94.0% and 99.7% at the resonant wavelengths of 422 and 545 nm, respectively. In addition, the optical properties of the proposed nanostructure can be tuned by the geometric parameters of the periodic Au nanocubes array, distributed Bragg mirror (DBR) and polarization angle of the incident light, which are of great pragmatic significance for improving the absorption efficiency and selectivity of monolayer MoS₂. The absorber is also able to withstand a wide range of incident angles, showing polarization-independence. Similar design ideas can also be implemented to other transition-metal dichalcogenides (TMDCs) to strengthen the interaction between light and MoS₂. This nanostructure is relatively simple to implement and has a potentially important application value in the development of high-efficiency solar energy absorbers and other optoelectronic devices.

Keywords: solar energy absorber; monolayer MoS₂; local surface plasmon resonances; Au nanocubes; transition-metal dichalcogenides

1. Introduction

As important energy collection devices, solar energy absorbers have attracted more and more attention in recent years [1–3]. For an ideal absorber, it is necessary to have a high light absorption and many other characteristics, such as polarization-dependence [4] and tunability [5]. However, problems arise as associated with limitations in low-temperature tolerance, low light absorption

efficiency, and materials [6–8]. Therefore, we need to propose a new type of broadband absorber based on materials with excellent physical properties to solve these existing problems.

Over the past few years, 2D materials, such as graphene and transition-metal dichalcogenides (TMDCs), have become the leading materials for numerous applications in modulators, optical detectors, metamaterial absorbers, and emitters due to their extraordinary electrical and optical characteristics, and also their ability to enhance light absorption with high temperature stability [9–25]. Researchers have a great interest in metamaterial absorbers due to their wide range of applications in energy harvesting, sensing, and photocatalysis [26–35]. Monolayer TMDCs are regarded as a kind of semiconductor material and have a direct bandgap at the *K* points of the Brillouin zone [36], which means only energy will change in the transition process while the momentum remains unchanged. This process only needs the participation of photons and does not require additional phonons, which makes it much easier to generate and has a higher quantum efficiency. Compared with pure graphene, TMDCs have been considered as more preferable materials for applications, because pure graphene's band-gap is zero [37] and its electrical conduction is only stimulated by electronic heat, which greatly limits its application in many fields. TMDCs have a tunable bandgap ranging from 1 to 2 eV [38], which provide opportunities for manufacturing photoelectron devices. Moreover, molybdenum disulfide (MoS₂) has been considered as one of the most promising materials for realizing functional photonic devices due to its high current cut-off ratios and tunable optoelectronic characteristics [39,40]. Monolayer MoS₂ shows excellent properties including direct band-gap and tunability, all of which are critical to optoelectronic devices manufacturing. However, due to its ultra-thin thickness, monolayer MoS₂ also faces an intractable challenge in weak light absorption, which would hinder its practical application. We know that the average absorption rate of monolayer MoS₂ is only 10% in the wavelength range from 450 to 800 nm [41]. Therefore, it is urgent to propose a useful method to improve the light absorption of monolayer MoS₂.

In the last decade, an increasing number of strategies have been proposed for light absorption enhancement of monolayer MoS₂. Based on the critical coupling mechanism, Xiao et al. [37] added an air chamber into a polymethyl methacrylate (PMMA)-SiO₂-Ag three-dimensional structure, which greatly enhanced the absorption of monolayer MoS₂. Hua et al. [42] enhanced Tamm Plasmon (TP) modes by inserting monolayer MoS₂ into a grid composed of titanium dioxide and silicon dioxide, and then enhanced its absorption to 96%. Janisch et al. [43] raised the absorption of MoS₂ to approximately 70% at 450 nm by using a nanocavity composed of alumina nano-layer spacers. Luo et al. [44] designed a perfect absorber based on metal-insulator-metal (MIM) metamaterial. The two absorption peaks of monolayer MoS₂ increased to 57% and 80.5%.

Additionally, a useful method of enhancing and remotely controlling the optical response of materials depends on the use of local surface plasmon resonances (LSPRs) maintained by metal nanoparticles (NPs) [45]. The LSPRs wavelength of silver and gold nanoparticles can be effectively adjusted by changing the size, shape, and surrounding medium [46,47]. Liu et al. [48] proposed embedded nanostructures of noble metal NPs. Theoretical analysis and experimental results show that the coupling effect of LSPRs on an electromagnetic field and ferromagnetic (FM) material will be greatly changed due to the position change of nanoparticles. Mehrvar et al. [49] enhanced Raman scattering by chemical deposition, using the combination of LSPRs for silver nanoparticles, longitudinal standing wave resonance of the silver layer, and interaction between particles in the gap region. Sobhani et al. [50] used Au-Shell nanoparticles with a surface coverage of less than 1% to enhance the photocurrent and photoluminescence effects of molybdenum disulfide. In this work, we choose representative Au NPs-Au nanocubes (NCs) for simulation. Although light absorption was promoted by the introduction of Au NCs, it is still insufficient to apply to solar energy absorbers and other optoelectronic devices. An effective strategy is urgently needed to tackle this problem.

In this paper, we proposed a new method to enhance the absorption of monolayer MoS₂ by using distributed Bragg mirror (DBR) as the substrate and combining with Au NCs periodic array nanostructures. DBR can effectively reduce light transmission and improve its reabsorption. Au NCs

will facilitate us to adjust the optical properties of the nanostructure. Thus, a new type of high-efficiency broadband solar energy absorber working in the visible band was obtained. Additionally, through our theoretical calculation, other TMDC materials besides MoS₂, such as WS₂, MoSe₂, and WSe₂, can also be used in this nanostructure. These results indicate that the plasmon-enhanced nanostructures have wide applicability in the efficient solar energy absorption of two-dimensional materials.

2. Structure and Theory

Figure 1 shows the nanostructure we proposed. The periodic Au NCs array, the DBR composed of SiO₂ and Si layers, and the monolayer MoS₂ between the periodic Au NCs array and the DBR constitute this nanostructure. In this work, the dielectric properties of MoS₂ were measured by Zhang et al. [51]. The Au NCs array is characterized by the period P_x and P_y in the x and y directions, respectively. The dielectric functions of SiO₂ and Si are derived from Palik [52]. The thickness of the monolayer SiO₂ layer is 90 nm and that of the Si layer is 38 nm. The incident optical source from air to the periodic Au NCs array is set for plane waves. The thickness of monolayer MoS₂ is 0.65 nm. The dielectric function of Au is derived from Palik [52]. Finite-difference time-domain (FDTD) simulation is used to calculate the light absorption of the proposed MoS₂-based nanostructure (Lumerical Solutions, Inc., Vancouver, YVR, Canada). Periodic boundary conditions are set around the unit cell, and the top and bottom boundaries of the cell are perfectly matched layer-absorbing boundary conditions. The formula for calculating absorption is $A = 1 - T - R$ [53–58]. T represents transmission and R represents reflection.

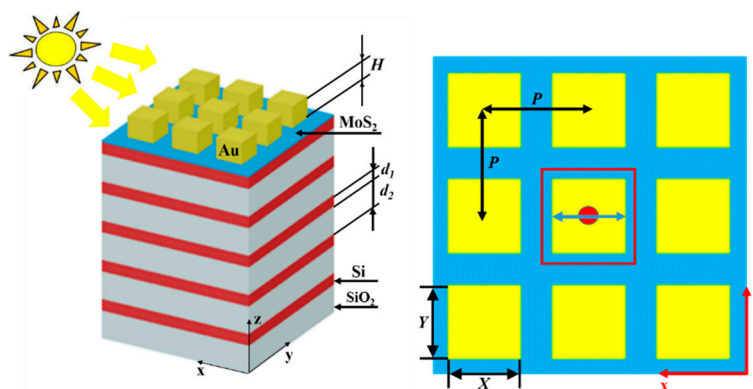


Figure 1. A schematic of the MoS₂-based nanostructure. X , Y , and H represent the length, width, and height of the nanocubes, respectively. d_1 and d_2 are the thickness of Si and SiO₂, respectively. P represents the period of the Au nanocubes (NCs) array.

3. Results and Discussions

In this paper, the geometric parameters of the structure are set as follows unless it is explicitly pointed out that the parameters have changed: $X = Y = H = 70$ nm, $N = 5$, $d_1 = 38$ nm, $d_2 = 90$ nm, and $P = 100$ nm. The simulated absorption spectra results of the monolayer MoS₂, a periodic Au NCs array, a periodic Au NCs array on monolayer MoS₂ and the proposed MoS₂-based nanostructure under transverse magnetic (TM)-polarized light are shown in Figure 2a. In the range of 400–700 nm visible light wavelength, the average absorptivity is about 0.1. The absorption at the peak of ~426 nm is about 0.29. Although the absorption coefficient of monolayer MoS₂ is large, which can be considered as a transparent medium particularly at the visible wavelength region because of its extremely thin thickness. As for the Au NCs array, the maximum absorptivity reaches about 0.64 at 400 nm because LSPRs mode is activated. For a periodic Au NCs array on monolayer MoS₂, the absorption is significantly enhanced compared with the monolayer MoS₂. The maximum absorption peak appears at ~424 nm with the absorption of 0.65, while the other two relatively low peaks are at 620 and 665 nm, with absorption peaks of 0.51 and 0.45, respectively. The absorption of the structure is obviously improved, but it is still too weak for practical applications.

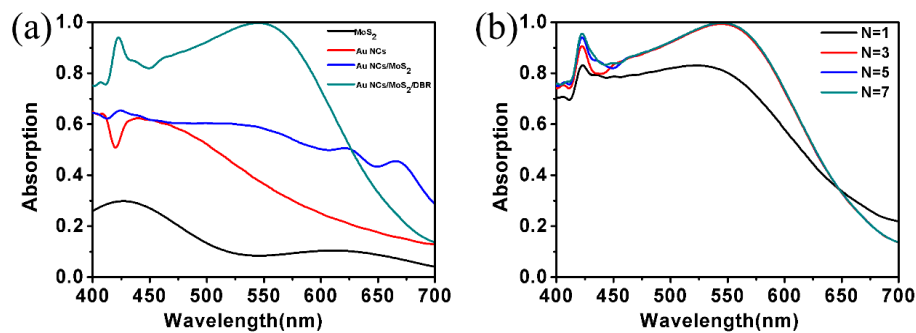


Figure 2. (a) Light absorption rate for Au NCs array, Au NCs/MoS₂, Au NCs/MoS₂/DBR, and monolayer MoS₂. (b) Light absorption rate for different period number N . DBR: distributed Bragg mirror.

Taking this into consideration, the DBR nanostructure in this work was supported. The DBR nanostructure serves as a reflector to reabsorb the reflected light, and the influence on the photoelectric figure of the equipment can be neglected. The transmission of the nanostructure, which is the DBR combined with the Au NCs array, will increase, and the absorption of the monolayer MoS₂ can be enhanced by the accomplishment of localized field concentration. It can be seen from the green line that the absorption is obviously improved due to the introduction of the DBR and the Au NCs array. The maximum absorption is above 0.99 from 533 to 554 nm, and another relatively low peak is above 0.94 at 422 nm.

Consequently, we investigated the influence of the period number N of DBR on the light absorption. With an increase in the period number of N , the absorption of nanostructures increases as shown in Figure 2b. When $N = 1$, the overall absorption is relatively low. The transmission of light is more obviously suppressed as the number N of DBR increases, thus improving light absorption. And the absorption will attain saturation when the period number $N \geq 5$. The optical reflectivity of the inserted DBR, which limits its continued enhancement of absorption, achieves a saturated value. That is the reason why the period number N was set as 5 in our calculation, which can maximize the absorption and is relatively simple to achieve.

Furthermore, the electric and magnetic influences on the two absorption peaks at the resonant wavelengths of 422 and 545 nm were investigated to explicate its physical mechanism. The distribution of electric field and magnetic field maps in a profile of the nanostructure under normal TM polarized light is shown in Figure 3a–d. As a result, the accumulation and the enhancement of electric and magnetic fields are clearly visible around the periphery of the Au nanocubes. In fact, the electromagnetic fields indicate such features due to the excitation of the LSPRs mode. MoS₂ has a good second-order nonlinear susceptibility because the space-reversal symmetry is broken, and that is the physical foundation for obtaining a high-intensity second harmonic. It is known that the internal exciton resonance effect can enhance the second harmonic intensity [59,60], and the enhanced second harmonic intensity is closely related to the electric and magnetic field enhancement caused by the LSPRs. Therefore, the combination of monolayer MoS₂ and an Au NCs array can enhance the absorption of monolayer MoS₂ and then the overall absorption of the proposed nanostructure. To conclude, LSPRs results in the accumulation of light energy, near-field enhancement, and limiting the incident electric and magnetic fields near the surface of the monolayer MoS₂ layer.

Next, it was found that the LSPRs frequency of Au NPs can be effectively adjusted by geometric parameters and the surrounding medium [61–63], hence the period of the Au NCs array, the X , Y , and H of the cube, and the incident angles of light were investigated. For our cubic structure, the principle of influencing optical properties by changing its geometrical parameters is similar to that of gold nanorods [64]. Figure 4a shows the influence of the period of the Au NCs array on the light absorption rate of the MoS₂-based nanostructure. When the period of the nanostructure increases from 90 to 130 nm, the absorption peak will appear at the shorter wavelength, which is due to the weakening of LSPRs between the Au NCs. With the increase of the period, the space between the nanocubes become

larger, and the energy localized around them decreases, which means more energy is radiating out. Finally, these factors lead to a blue-shift. However, the overall peak does not change significantly, which provides possibilities for the operation of optoelectronic devices at different frequencies. Figure 4b demonstrates the effect of Y on the absorption spectra (here, we set $X = H = 70$ nm). It can be seen that there is no obvious change in the absorption spectra as a whole. This is because the magnetic field of TM-polarized light is perpendicular to the x - z plane and the change of the length of Y has little effect on absorption, which means that the resonant wavelength is not susceptible to Y . Subsequently, we then investigated the effects of X on the absorption spectra (Y and H are fixed as 70 nm). The results are shown in Figure 4c. Altering X from 40 to 90 nm, the effective resonant wavelength of LSPRs mode will increase, so the resonance peak would be obviously red-shifted from 454 to 685 nm. When $X = 70$ nm, the overall absorption rate achieves optimal value.

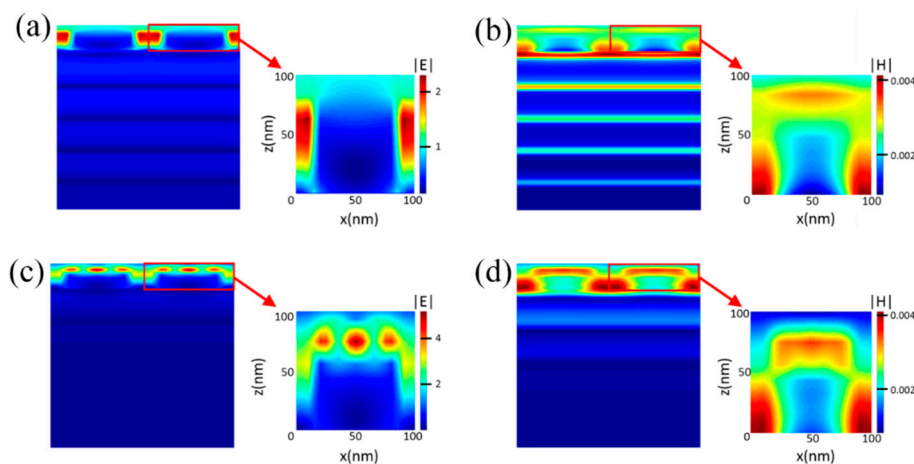


Figure 3. Electric field and magnetic field maps of the proposed MoS₂-based nanostructure under TM-polarized light incidence. (a,b) represent the electric field and magnetic field maps at 422 nm. (c,d) represent the electric field and magnetic field maps at 545 nm.

We then took the impacts of height (H) of the cubes on the absorptivity of monolayer MoS₂ (X and Y are fixed as 70 nm) into account, as shown in Figure 4d. When the H is 70 nm, the peak value reaches a maximum of 0.99. Taking all the factors mentioned above into consideration, we finally decided to set $X = Y = Z = 70$ nm in this work.

In addition, the effect of the polarization angle θ (θ is the angle between the plane wave and the X -axis) on structure absorption was discussed, as shown in Figure 5. It can be found that when the θ varies from 0° to 90° , the absorption peak blue-shifts from 607 to 544 nm. To understand the optical properties of the discussed polarization direction for the nanostructure, we simulated the electric field distributions (X - Y plane) on the surface (between the Au nanocubes and the monolayer MoS₂) of the nanostructure, as illustrated in Figure 6. In Figure 6, the incident light is polarized along the X -axis (TM-polarized light). The θ increases from 0° to 90° and the electric field distributions of the cubes' LSPRs excitation mode gradually changed from longitudinal dominance to transverse dominance, which is the main reason for the blue-shift of the absorption peak.

Furthermore, we illustrated the absorption spectra at various incident angles for transverse electric (TE) and TM polarizations. As is widely known, in the pragmatic application of solar energy absorber, the ideal equipment should meet the requirements of high light absorption to adapt to a relatively large range of incident angles. The results are shown in Figure 7. When increasing the incident angle from 0° to 45° , the absorption peaks remained relatively stable, whether for TM or TE polarization, which means that both for TM or TE polarization, the absorption of monolayer MoS₂ in the nanostructures can be significantly enhanced. This is because TM or TE polarized light with a small incident angle can keep LSPRs coupling. This provides a very suitable method for optimizing the absorption in the

visible wavelength region by altering the incident angle. As a result, the combination of polarization insensitivity and excellent absorption stability at oblique incidence makes this kind of absorber more feasible in the pragmatic application of solar energy absorption [65–68].

In order to explore the value of the absorber in practical application, the solar energy absorption response of the proposed structure was studied. The results are shown in Figure 8. It can be observed that the proposed nanostructure exhibits a superior absorption performance for sunlight at the visible wavelength region under the solar source of Air Mass (AM) 1.5. As we can see from Figure 8, the average absorption can reach 90.5% at the wavelength range from 430 to 630 nm. Even in the whole region near the wavelength width of visible light, the average absorption is about 77.3%. Compared with several kinds of previous absorbers, there are many advantages in this work, as shown in Table 1. The average absorption rate of the proposed absorber is the highest and the range of the working area is also the widest, while the performance of other absorbers is somewhat inferior. The above researches confirm our assumption that the proposed nanostructure will absorb energy highly in the visible band of solar radiation.

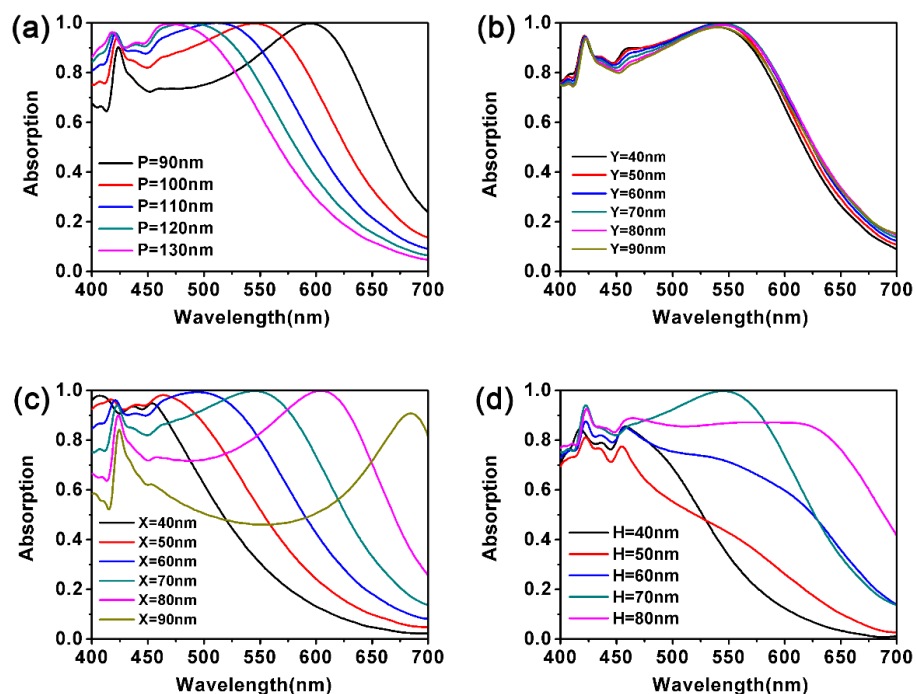


Figure 4. (a–d) Effects of different geometric parameters. The four pictures represent (a) the period of Au NCs array, (b) edge Y parallel to Y-axis, (c) edge X parallel to X-axis, and (d) the height H of the Au NCs.

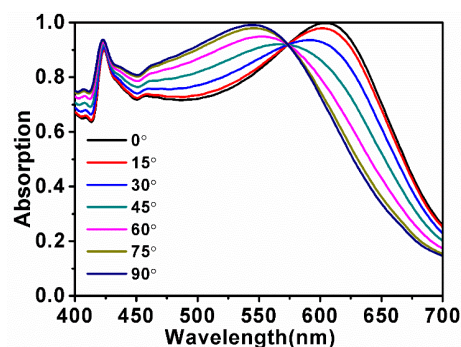


Figure 5. Absorption spectra with a different polarization direction (θ). Y and H are set as 70 nm and X is set as 80 nm. The θ increases from 0° to 90° .

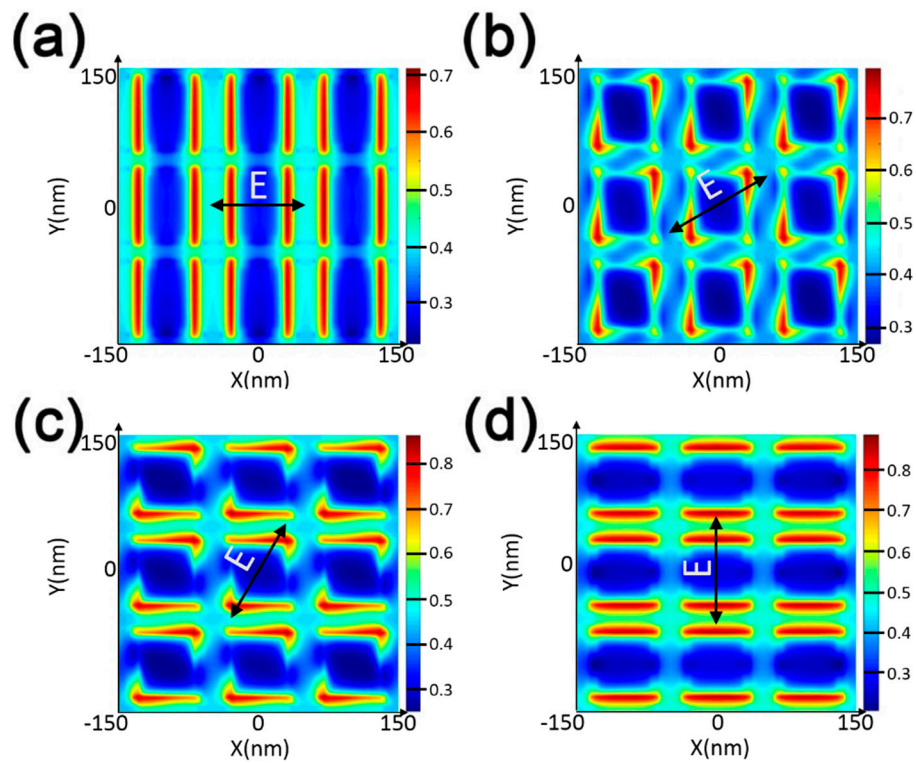


Figure 6. Electric field distributions (X–Y plane) on the surface for (a) $\theta = 0^\circ$, (b) $\theta = 30^\circ$, (c) $\theta = 60^\circ$, and (d) $\theta = 90^\circ$.

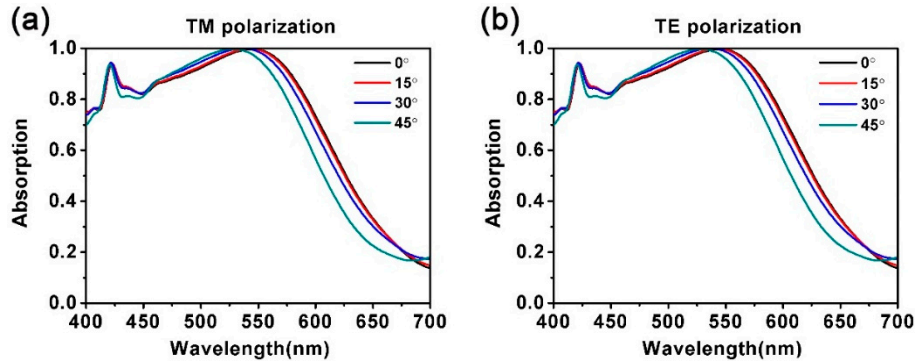


Figure 7. Influence of the incident angle on the absorption spectra for (a) TM polarization and (b) TE polarization.

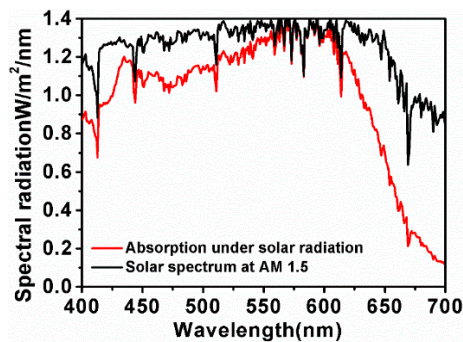


Figure 8. Absorption spectrum for the MoS₂-based nanostructure absorber under a solar spectrum at AM 1.5.

Table 1. Comparison of several latest absorbers with the absorbers we have proposed. (quantum dots (QDs); metal-insulator-metal (MIM); graphene-molybdenum disulfide photovoltaic cells (GM-PVC); wedge-shaped metal-mirror microcavities (w-MMCs))

Absorber	Average Absorption (%)	Operating Region(nm)
Graphene/MoS ₂ Interface [69]	15.4%	Absorption is always less than 75%
QDs/MoS ₂ /SiO ₂ /Si [70]	22.3%	Absorption is always less than 75%
Monolayer MoS ₂ with MIM [44]	Less than 50%	500–750
GM-PVC in w-MMCs [71]	65%	450–700
Proposed (monolayer MoS ₂ /Au NCs/DBR)	77.3%	400–700, absorbance is more than 90.4% from 430 to 630 nm

Finally, the proposed nanostructure was used to enhance the light absorption rate of other TMDCs, such as WS₂, MoSe₂, and WSe₂, where MoS₂ is displaced by other TMDCs in the proposed nanostructures. The light absorption rate for our proposed nanostructure of monolayer WS₂, MoSe₂ and WSe₂ are shown in Figure 9a–c. The data for WS₂, MoSe₂ and WSe₂ is obtained from Jiang et al. [37]. The selected geometric parameters are exactly the same as the proposed MoS₂-based nanostructure. It can be seen that the absorption of these materials has been greatly enhanced by the nanostructure, too. The similarity between these three materials and MoS₂ leads to this result, which also means that the operating wavelength can be changed by altering the geometric parameters mentioned above. It should be pointed out that due to the different corresponding imaginary parts of the dielectric constants of these three materials in close proximity to the resonance wavelength, different absorption losses are caused, resulting in slightly different absorption rates. Additionally, under the simulated solar irradiation, these three materials also show excellent solar energy absorption properties, as shown in Figure 10a–c. In conclusion, our proposed TMDCs-based nanostructure provides a theoretical basis for enhancing the solar energy absorption of other monolayer TMDCs materials.

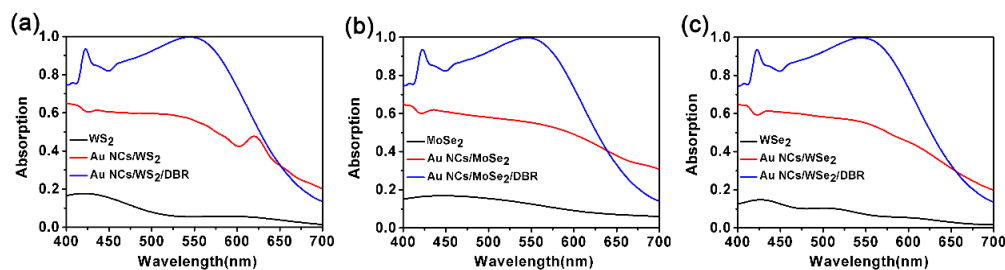


Figure 9. Light absorption rate of monolayer (a) WS₂, (b) MoSe₂ and (c) WSe₂ in our nanostructures. The light absorption rate of Au NCs/TMDCs/DBR, Au NCs/TMDCs and monolayer TMDCs is shown in the figure as a comparison. $X = Y = H = 70$ nm, $P = 100$ nm, $d_1 = 38$ nm, $d_2 = 90$ nm, and $N = 5$. TMDCs: transition-metal dichalcogenides.

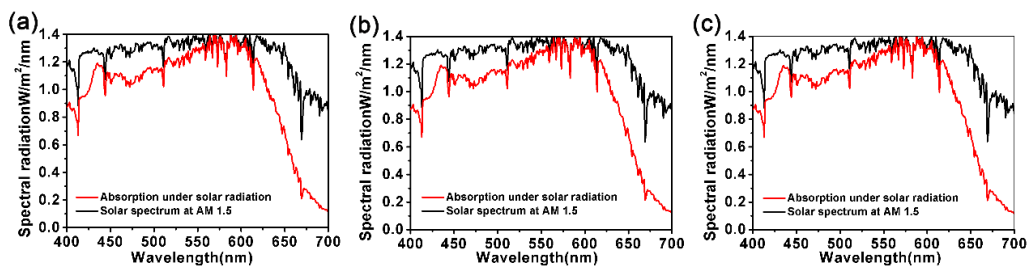


Figure 10. Absorption spectra of monolayers (a) WS₂, (b) MoSe₂, and (c) WSe₂ introduced into our nanostructure absorber under a solar spectrum at AM 1.5.

4. Conclusions

A novel nanostructure composed of a periodic Au NCs array and distributed Bragg mirror (DBR) for a monolayer MoS₂ was proposed to enhance LSPRs. By theoretical calculations, it was demonstrated that the combination of a monolayer MoS₂ with an Au NCs array and a DBR provides a theoretical basis for the development of a perfect solar energy absorber with high-temperature stability, high absorptivity, and easy implementation. Under solar radiation, the absorption spectra generated by the absorber is well-matched with the energy distribution in the solar visible band. The light absorption rates of the proposed MoS₂-based absorbers are more than 94.0% and 99.7% at the resonant wavelengths of 422 and 545 nm, respectively. Further studies show that the absorption of MoS₂-based nanostructures can be flexibly adjusted by changing the geometric parameters and the polarization degrees of the incident light. This method has an important practical significance for improving the absorption efficiency and selectivity of monolayer MoS₂. The proposed MoS₂-based nanostructures can also be used for both TM and TE polarizations. Similar results can be obtained by other TMDCs, such as WS₂, MoSe₂, and WSe₂. This will provide references for the design of other solar energy absorbers and optoelectronic devices based on TMDCs. The proposed structure will promote the areas of absorption efficiency, tunability and polarization-independence of solar energy absorbers once the large-scale fabrication techniques of such materials become more feasible in the future.

Author Contributions: Conceptualization, J.L., Z.C., and Z.Y.; data curation, J.L., Z.C., and X.C.; formal analysis, Z.Y., W.Y., T.D., P.W., and H.Y.; methodology, H.Y., G.L., and Y.Y.; resources, P.W.; software, P.W., Z.C., Y.Y., X.C., and G.L.; data curation, J.L.; writing—original draft preparation, J.L.; writing—review and editing, J.L., Z.C., Z.Y., W.Y., and Y.Y. All authors have read and agreed to the published version of the manuscript.

Funding: This research was funded by the National Natural Science Foundation of China (NNSFC), grant numbers 51606158, 11604311, 61705204, 21506257, 11604091, 11547186, and 51575407; funded by the Natural Science Foundation of Fujian Province, grant numbers 2018J05008 and JZ160459; funded by the Sichuan Science and Technology Program, grant number 2018GZ0521; Funded by the PhD Research Startup Foundation of Quanzhou Normal University (G16057); and funded by the Distinguished Young Scholars Program of Fujian Province (C18032).

Conflicts of Interest: The authors declare no conflicts of interest.

References

1. Liu, Z.Q.; Liu, G.Q.; Huang, Z.P.; Liu, X.S.; Fu, G.L. Ultra-broadband perfect solar absorber by an ultra-thin refractory titanium nitride meta-surface. *Sol. Energy Mater. Sol. Cell.* **2018**, *179*, 346–352. [[CrossRef](#)]
2. Yu, P.Q.; Chen, X.F.; Yi, Z.; Tang, Y.J.; Yang, H.; Zhou, Z.G.; Duan, T.; Cheng, S.B.; Zhang, J.G.; Yi, Y.G. A numerical research of wideband solar absorber based on refractory metal from visible to near infrared. *Opt. Mater.* **2019**, *97*, 109400. [[CrossRef](#)]
3. Liang, C.P.; Zhang, Y.B.; Yi, Z.; Chen, X.F.; Zhou, Z.G.; Yang, H.; Yi, Y.; Tang, Y.J.; Yao, W.T.; Yi, Y.G. A broadband and polarization-independent metamaterial perfect absorber with monolayer Cr and Ti elliptical disks array. *Results Phys.* **2019**, *15*, 102635. [[CrossRef](#)]
4. Wu, P.H.; Chen, Z.Q.; Xu, D.Y.; Zhang, C.F.; Jian, R.H. A narrow dual-band monolayer unpatterned graphene-based perfect absorber with critical coupling in the near infrared. *Micromachines* **2020**, *11*, 58. [[CrossRef](#)]
5. Wu, P.H.; Chen, Z.Q.; Jile, H.; Zhang, C.F.; Xu, D.Y.; Lv, L. An Infrared Perfect Absorber Based on Metal-Dielectric-Metal Multi-layer Films with Nanocircle Holes Arrays. *Results Phys.* **2020**, *16*, 102952. [[CrossRef](#)]
6. Wang, Y.Y.; Chen, Z.Q.; Xu, D.Y.; Yi, Z.; Chen, X.F.; Chen, J.; Tang, Y.J.; Wu, P.H.; Li, G.F.; Yi, Y.G. Triple-band perfect metamaterial absorber with good operating angle polarization tolerance based on split ring arrays. *Results Phys.* **2020**, *16*, 102951. [[CrossRef](#)]
7. Cheng, Z.Z.; Cheng, Y.Z. A multi-functional polarization convertor based on chiral metamaterial for terahertz waves. *Opt. Commun.* **2019**, *435*, 178–182. [[CrossRef](#)]
8. Liu, E.; Tan, W.; Yan, B.; Xie, J.; Ge, R.; Liu, J. Broadband ultra-flattened dispersion, ultra-low confinement loss and large effective mode area in an octagonal photonic quasi-crystal fiber. *J. Opt. Soc. Am. A* **2018**, *35*, 431–436. [[CrossRef](#)]

9. Cen, C.L.; Chen, Z.Q.; Xu, D.Y.; Jiang, L.Y.; Chen, X.F.; Yi, Z.; Wu, P.H.; Li, G.F.; Yi, Y.G. High quality factor, high sensitivity metamaterial graphene-perfect absorber based on critical coupling theory and impedance matching. *Nanomaterials* **2020**, *10*, 95. [[CrossRef](#)]
10. Wang, Y.Y.; Qin, F.; Yi, Z.; Chen, X.F.; Zhou, Z.G.; Yang, H.; Liao, X.; Tang, Y.J.; Yao, W.T.; Yi, Y.G. Effect of slit width on surface plasmon resonance. *Results Phys.* **2019**, *15*, 102711. [[CrossRef](#)]
11. Cen, C.L.; Zhang, Y.B.; Chen, X.F.; Yang, H.; Yi, Z.; Yao, W.T.; Tang, Y.J.; Yi, Y.G.; Wang, J.Q.; Wu, P.H. A dual-band metamaterial absorber for graphene surface plasmon resonance at terahertz frequency. *Phys. E* **2020**, *117*, 113840. [[CrossRef](#)]
12. Fang, R.; Miao, C.; Mou, H.Y.; Xiao, W. Facile synthesis of Si@TiO₂@rGO composite with sandwich-like nanostructure as superior performance anodes for lithium ion batteries. *J. Alloys Compd.* **2020**, *818*, 152884. [[CrossRef](#)]
13. Huo, Z.; Liu, E.; Liu, J. Hollow-core photonic quasicrystal fiber with high birefringence and ultra-low nonlinearity. *Chin. Opt. Lett.* **2020**, *18*, 030603.
14. Qi, Y.P.; Zhou, P.Y.; Zhang, T.; Zhang, X.W.; Wang, Y.; Liu, C.Q.; Bai, Y.L.; Wang, X.X. Theoretical study of a multichannel plasmonic waveguide notch filter with double-sided nanodisk and two slot cavities. *Results Phys.* **2019**, *15*, 102506. [[CrossRef](#)]
15. Qi, Y.P.; Liu, C.Q.; Hu, B.B.; Deng, X.Y.; Wang, X.X. Tunable plasmonic absorber in THz-band range based on graphene “arrow” shaped metamaterial. *Results Phys.* **2019**, *15*, 102777. [[CrossRef](#)]
16. Qi, Y.P.; Wang, Y.; Zhang, X.W.; Liu, C.Q.; Hu, B.B.; Bai, Y.L.; Wang, X.X. A theoretical study of optically enhanced transmission characteristics of subwavelength metal Y-shaped arrays and its application on refractive index sensor. *Results Phys.* **2019**, *15*, 102495. [[CrossRef](#)]
17. Liu, Z.Q.; Tang, P.; Wu, B.; Shi, L.L.; Li, Y.Y.; Liu, X.S. Split graphene nano-disks with tunable, multi-band, and high-Q plasmon modes. *Opt. Mater.* **2019**, *89*, 18–24. [[CrossRef](#)]
18. Liu, X.; Liu, G.; Tang, P.; Fu, G.; Du, G.; Chen, Q.; Liu, Z. Quantitatively optical and electrical-adjusting high-performance switch by graphene plasmonic perfect absorbers. *Carbon* **2018**, *140*, 362–367. [[CrossRef](#)]
19. Wang, X.X.; Wu, X.X.; Zhu, J.K.; Pang, Z.Y.; Yang, H.; Qi, Y.P. Theoretical investigation of a highly sensitive refractive-index sensor based on TM₀ waveguide mode resonance excited in an asymmetric metal-cladding dielectric waveguide structure. *Sensors* **2019**, *19*, 1187. [[CrossRef](#)]
20. Liu, C.; Yang, L.; Lu, X.L.; Liu, Q.; Wang, F.M.; Lv, J.W.; Sun, T.; Mu, H.W.; Chu, P.K. Mid-infrared surface plasmon resonance sensor based on photonic crystal fibers. *Opt. Express* **2017**, *25*, 14227–14237. [[CrossRef](#)]
21. Liu, Q.; Yan, B.; Liu, J. U-shaped photonic quasi-crystal fiber sensor with high sensitivity based on surface plasmon resonance. *Appl. Phys. Express* **2019**, *12*, 052014. [[CrossRef](#)]
22. Li, M.W.; Liang, C.P.; Zhang, Y.B.; Yi, Z.; Chen, X.F.; Zhou, Z.G.; Yang, H.; Tang, Y.J.; Yi, Y.G. Terahertz wideband perfect absorber based on open loop with cross nested structure. *Results Phys.* **2019**, *15*, 102603. [[CrossRef](#)]
23. Cheng, Y.Z.; Fan, J.P.; Luo, H.; Chen, F. Dual-band and high-efficiency circular polarization convertor based on anisotropic metamaterial. *IEEE Access* **2020**, *8*, 7615–7621. [[CrossRef](#)]
24. Cai, C.; Han, S.B.; Liu, W.; Sun, K.; Qiao, L.; Li, S.; Zu, X.T. Tuning catalytic performance by controlling reconstruction process in operando condition. *Appl. Catal. B* **2020**, *260*, 118103. [[CrossRef](#)]
25. Li, W.Y.; Cheng, Y.Z. Dual-band tunable terahertz perfect metamaterial absorber based on strontium titanate (STO) resonator structure. *Opt. Commun.* **2020**, *462*, 125265. [[CrossRef](#)]
26. Yan, Y.X.; Yang, H.; Yi, Z.; Xian, T. NaBH₄ reduction induced evolution of Bi nanoparticles from BiOCl nanoplates and construction of promising Bi@BiOCl hybrid photocatalysts. *Catalysts* **2019**, *9*, 795. [[CrossRef](#)]
27. Wang, Y.P.; Yang, H.; Sun, X.F.; Zhang, H.M.; Xian, T. Preparation and photocatalytic application of ternary n-BaTiO₃/Ag/p-AgBr heterostructured photocatalysts for dye degradation. *Mater. Res. Bull.* **2020**, *124*, 110754. [[CrossRef](#)]
28. Guan, S.T.; Yang, H.; Sun, X.F.; Xian, T. Preparation and promising application of novel LaFeO₃/BiOBr heterojunction photocatalysts for photocatalytic and photo-Fenton removal of dyes. *Opt. Mater.* **2020**, *100*, 109644. [[CrossRef](#)]
29. Yan, Y.X.; Yang, H.; Yi, Z.; Xian, T.; Wang, X.X. Direct Z-scheme CaTiO₃@BiOBr composite photocatalysts with enhanced photodegradation of dyes. *Sci. Pollut. Res.* **2019**, *26*, 29020–29031. [[CrossRef](#)]
30. Wang, Y.P.; Jiang, F.C.; Chen, J.F.; Sun, X.F.; Xian, T.; Yang, H. In situ construction of CNT/CuS hybrids and their application in photodegradation for removing organic dyes. *Nanomaterials* **2020**, *10*, 178. [[CrossRef](#)]
31. Yan, Y.X.; Yang, H.; Yi, Z.; Li, R.S.; Xian, T. Design of ternary CaTiO₃/g-C₃N₄/AgBr Z-scheme heterostructured photocatalysts and their application for dye photodegradation. *Solid State Sci.* **2020**, *100*, 106102. [[CrossRef](#)]

32. Yi, Z.; Li, X.; Wu, H.; Chen, X.F.; Yang, H.; Tang, Y.J.; Yi, Y.G.; Wang, J.Q.; Wu, P.H. Fabrication of ZnO@Ag₃PO₄ Core-Shell nanocomposite arrays as photoanodes and their photoelectric properties. *Nanomaterials* **2019**, *9*, 1254. [[CrossRef](#)] [[PubMed](#)]
33. Yi, Z.; Zeng, Y.; Wu, H.; Chen, X.F.; Fan, Y.X.; Yang, H.; Tang, Y.J.; Yi, Y.G.; Wang, J.Q.; Wu, P.H. Synthesis, surface properties, crystal structure and dye-sensitized solar cell performance of TiO₂ nanotube arrays anodized under different parameters. *Results Phys.* **2019**, *15*, 102609. [[CrossRef](#)]
34. Li, G.F.; Li, J.H.; Ju, Z.J.; Sun, Y.; Kong, J.Y. A novel feature extraction method for machine learning based on surface electromyography from healthy brain. *Neural Comput. Appl.* **2019**, *31*, 9013–9022. [[CrossRef](#)]
35. Li, G.F.; Zhang, L.L.; Sun, Y.; Kong, J.Y. Towards the semg hand: Internet of things sensors and haptic feedback application. *Multimed. Tools Appl.* **2019**, *78*, 29765–29782. [[CrossRef](#)]
36. Jiang, P.; Song, G.; Wang, Y.L.; Li, C.; Wang, L.L.; Yu, L. Tunable strong exciton–plasmon–exciton coupling in WS₂–J-aggregates–plasmonic nanocavity. *Opt. Express* **2019**, *27*, 16613–16623. [[CrossRef](#)]
37. Jiang, X.; Wang, T.; Xiao, S.; Yan, X.; Cheng, L.; Zhong, Q. Approaching perfect absorption of monolayer molybdenum disulfide at visible wavelengths using critical coupling. *Nanotechnology* **2018**, *29*, 335205. [[CrossRef](#)]
38. Jiang, D.; Li, G.F.; Sun, Y.; Kong, J.Y.; Tao, B. Gesture recognition based on skeletonization algorithm and CNN with ASL database. *Multimed. Tools Appl.* **2019**, *78*, 29953–29970. [[CrossRef](#)]
39. Li, Y.; Liu, Z.; Zhang, H.; Tang, P.; Wu, B.; Liu, G. Ultra-broadband perfect absorber utilizing refractory materials in metal-insulator composite multilayer stacks. *Opt. Express* **2019**, *27*, 11809–11818. [[CrossRef](#)]
40. Chen, J.; Fan, W.F.; Zhang, T.; Chen, X.Y.; Wu, J.J.; Li, D.Y.; Yu, Y. Engineering the magnetic plasmon resonances of metamaterials for high-quality sensing. *Opt. Express* **2017**, *25*, 3675–3681. [[CrossRef](#)]
41. Luo, X.; Liu, Z.M.; Cheng, Z.Q.; Liu, J.P.; Lin, Q.; Wang, L.L. Polarization-insensitive and wide-angle broadband absorption enhancement of molybdenum disulfide in the visible regime. *Opt. Express* **2018**, *26*, 33918–33929. [[CrossRef](#)] [[PubMed](#)]
42. Lu, H.; Gan, X.; Mao, D.; Fan, Y.; Zhao, J. Nearly perfect absorption of light in monolayer molybdenum disulfide supported by multilayer structures. *Opt. Express* **2017**, *25*, 21630–21636. [[CrossRef](#)] [[PubMed](#)]
43. Janisch, C.; Song, H.; Zhou, C.; Lin, Z. MoS₂ monolayers on nanocavities: Enhancement in light–matter interaction. *2D Mater.* **2016**, *3*, 025017. [[CrossRef](#)]
44. Luo, X.; Zhai, X.; Wang, L.L.; Lin, Q. Enhanced dual-band absorption of molybdenum disulfide using a plasmonic perfect absorber. *Opt. Express* **2018**, *26*, 11658–11666. [[CrossRef](#)]
45. Wang, X.X.; Zhu, J.K.; Wen, X.L.; Wu, X.X.; Wu, Y.; Su, Y.W.; Tong, H.; Qi, Y.P.; Yang, H. Wide range refractive index sensor based on a coupled structure of Au nanocubes and Au film. *Opt. Mater. Express* **2019**, *9*, 3079–3088. [[CrossRef](#)]
46. Qin, F.; Chen, Z.Q.; Chen, X.F.; Yi, Z.; Yao, W.T.; Duan, T.; Wu, P.H.; Yang, H.; Li, G.F.; Yi, Y.G. A Tunable Triple-Band Near-Infrared Metamaterial Absorber Based on Au Nano-Cuboids Array. *Nanomaterials* **2020**, *10*, 207. [[CrossRef](#)]
47. Zhou, K.; Song, J.L.; Lu, L.; Luo, Z.X.; Cheng, Q. Plasmon-enhanced broadband absorption of MoS₂-based structure using Au nanoparticles. *Opt. Express* **2019**, *27*, 2305–2316. [[CrossRef](#)]
48. Hou, T.; Ge, R.; Tan, W.; Liu, J. One-way rotating state of multi-periodicity frequency bands in circular photonic crystal. *J. Phys. D Appl. Phys.* **2020**, *53*, 075104. [[CrossRef](#)]
49. Mehrvar, L.; Sadeghipari, M.; Tavassoli, S.; Mohajerzadeh, S.; Fathipour, M. Optical and surface enhanced Raman scattering properties of Ag modified silicon double nanocone array. *Sci. Rep.* **2017**, *7*, 12106. [[CrossRef](#)]
50. Sobhani, A.; Lauchner, A.; Najmaei, S.; Ayala-Orozco, C.; Wen, F.; Lou, J. Enhancing the photocurrent and photoluminescence of single crystal monolayer MoS₂ with resonant plasmonic nanoshells. *Appl. Phys. Lett.* **2014**, *104*, 031112. [[CrossRef](#)]
51. Zhang, H.; Ma, Y.; Wan, Y.; Rong, X.; Xie, Z.; Wang, W. Measuring the refractive index of highly crystalline monolayer MoS₂ with high confidence. *Sci. Rep.* **2015**, *5*, 8440. [[CrossRef](#)] [[PubMed](#)]
52. Palik, E.D. *Handbook of Optical Constants of Solids II*; Academic Press: Boston, MA, USA, 1991; pp. 77–135.
53. Liu, E.; Yan, B.; Tan, W.; Xie, J.; Ge, R.; Liu, J. Guiding characteristics of Sunflower-type fiber. *Superlattices Microstruct.* **2018**, *115*, 123–129. [[CrossRef](#)]
54. Kou, Z.Y.; Miao, C.; Mei, P.; Zhang, Y.; Yan, X.M.; Jiang, Y.; Xiao, W. Enhancing the cycling stability of all-solid-state lithium-ion batteries assembled with Li_{1.3}Al_{0.3}Ti_{1.7}(PO₄)₃ solid electrolytes prepared from precursor solutions with appropriate pH values. *Ceram. Int.* **2020**. [[CrossRef](#)]

55. Liu, C.; Yang, L.; Liu, Q.; Wang, F.M.; Sun, Z.J.; Sun, T.; Mu, H.W.; Chu, P.K. Analysis of a surface plasmon resonance probe based on photonic crystal fibers for low refractive index detection. *Plasmonics* **2018**, *13*, 779–784. [[CrossRef](#)]
56. Shi, D.; Xiong, Z.; Li, J.; Luo, B.; Fang, L.; Xia, Y.; Gao, Z. Electron transition and electron-hole recombination processes in epitaxial BaTiO₃ films with embedded Co nanocrystals. *Mater. Res. Express* **2019**, *6*, 105021. [[CrossRef](#)]
57. Xiong, Z.; Cao, L. High magnetic-dielectric tunability in Ni nanocrystals embedded BaTiO₃ films. *J. Alloys Compd.* **2019**, *785*, 200–205. [[CrossRef](#)]
58. Qi, Y.P.; Zhang, X.W.; Zhou, P.Y.; Hu, B.B.; Wang, X.X. Refractive index sensor and filter of metal-insulator-metal waveguide based on ring resonator embedded by cross structure. *Acta Phys. Sin.* **2018**, *67*, 197301.
59. Sun, J.H.; Gu, Y.J.; Lei, D.Y.; Lau, S.P.; Wong, W.T.; Wong, K.Y. Mechanistic understanding of excitation-correlated nonlinear optical properties in MoS₂ nanosheets and nanodots: The role of exciton resonance. *ACS Photonics* **2016**, *3*, 2434–2444. [[CrossRef](#)]
60. Wang, G.; Marie, X.; Gerber, I. Giant enhancement of the optical second-harmonic emission of WSe₂ monolayers by laser excitation at exciton resonances. *Phys. Rev. Lett.* **2015**, *114*, 097403. [[CrossRef](#)]
61. Zhang, X.W.; Qi, Y.P.; Zhou, P.Y.; Gong, H.H.; Hu, B.B.; Yan, C.M. Refractive Index Sensor Based on Fano Resonances in Plasmonic Waveguide With Dual Side-Coupled Ring Resonators. *Photonic Sens.* **2018**, *8*, 367–374. [[CrossRef](#)]
62. Liang, C.P.; Yi, Z.; Chen, X.F.; Tang, Y.J.; Yi, Y.; Zhou, Z.G.; Wu, X.G.; Huang, Z.; Yi, Y.G.; Zhang, G.F. Dual-band infrared perfect absorber based on a Ag-dielectric-Ag multilayer films with nanoring grooves arrays. *Plasmonics* **2020**, *15*, 93–100. [[CrossRef](#)]
63. Liao, M.; Wu, L.F.; Zhang, Q.B.; Dai, J.Y.; Yao, W.T. Controlled morphology of single-crystal molybdenum trioxide nanobelts for photocatalysis. *J. Nanosci. Nanotechnol.* **2020**, *20*, 1917–1921. [[CrossRef](#)] [[PubMed](#)]
64. Liu, C.; Fu, G.L.; Wang, F.M.; Yi, Z.; Xu, C.H.; Yang, L.; Liu, Q.; Liu, W.; Li, X.L.; Mu, H.W.; et al. Ex-centric core photonic crystal fiber sensor with gold nanowires based on surface plasmon resonance. *OPTIK* **2019**, *196*, 163173. [[CrossRef](#)]
65. Fan, J.P.; Cheng, Y.Z. Broadband high-efficiency cross-polarization conversion and multi-functional wavefront manipulation based on chiral structure metasurface for terahertz wave. *J. Phys. D: Appl. Phys.* **2020**, *53*, 025109. [[CrossRef](#)]
66. He, X.K.; Sun, Z.Y.; Zou, Q.T.; Yang, J.J.; Wu, L.Y. Codeposition of nanocrystalline Co-Ni catalyst based on 1-ethyl-3-methylimidazolium bisulfate and ethylene glycol system for hydrogen evolution reaction. *J. Electrochem. Soc.* **2019**, *166*, D908–D915. [[CrossRef](#)]
67. Li, R.; Miao, C.; Zhang, M.Q.; Xiao, W. Novel hierarchical structural SnS₂ composite supported by biochar carbonized from chewed sugarcane as enhanced anodes for lithium ion batteries. *Ionics* **2019**. [[CrossRef](#)]
68. Zou, H.; Cheng, Y. Design of a six-band terahertz metamaterial absorber for temperature sensing application. *Opt. Mater.* **2019**, *88*, 674–679. [[CrossRef](#)]
69. Marco, B.; Palummo, M.; Grossman, J.C. Extraordinary sunlight absorption and one nanometer thick photovoltaics using two-dimensional monolayer materials. *Nano Lett.* **2013**, *13*, 3664–3670.
70. Mukherjee, B.; Guchhait, A.; Chan, Y.; Simsek, E. Absorptance of PbS quantum dots thin film deposited on trilayer MoS₂. *Adv. Mater. Lett.* **2015**, *6*, 936–940. [[CrossRef](#)]
71. Liu, J.; Cao, Y.; Tong, H.; Wang, D.; Wu, Z. Broad-spectrum enhanced absorption of graphene-molybdenum disulfide photovoltaic cells in metal-mirror microcavity. *Nanotechnology* **2018**, *29*, 144001.

